THE ASTRONOMICAL JOURNAL VOLUME 111, NUMBER 3 MARCH 1996

EMBEDDED CLUSTERS IN GIANT EXTRAGALACTIC H II REGIONS. III. EXTINCTION AND STAR FORMATION

Y. D. MAYYA[1] AND T. P. PRABHU

Indian Institute of Astrophysics, Bangalore 560 034, India
Electronic mail: ydm@tifrvax.tifr.res.in and tpp@iiap.ernet.in

Received 1994 December 7; revised 1995 December 13

ABSTRACT

A study of star formation is carried out on 35 giant extragalactic H II regions (GEHRs) in seven galaxies using optical photometric data in BVR broad bands and in the emission line of Hα. Interstellar extinction, metallicity and nebular contributions to the broad bands are estimated using spectroscopic data on these objects. Dimensionless diagrams involving $B-V$ and $V-R$ colors and the flux ratio of Balmer line to B band continuum are used to study star formation. The cluster colors indicate reduced extinction towards stellar continuum compared to the values derived from Balmer lines for the ionized gas. The frequency of detection of classical young ($t<3$ Myr) regions with only one burst of star formation is found to be low as compared to young regions with an accompanying population rich in red supergiants from a previous burst ($t\sim 10$ Myr). Reduced extinction towards cluster stars, destruction of ionizing photons and the existence of older population, often spatially unresolvable from the younger population, all conspire to make the observed Balmer line equivalent widths low in a majority of the GEHRs. A scenario of star formation is suggested which explains many of the observed properties of GEHRs, including the core-halo structure, reduced extinction for the radiation from stars as compared to that from the nebular gas, non-detection of young single burst regions and the co-existence of two populations of different ages. © *1996 American Astronomical Society.*

1. INTRODUCTION

Giant extragalactic H II regions (GEHRs) are sites of current star formation activity in galactic disks. A detailed investigation of star formation in these relatively simpler systems is important towards understanding star formation in more complex star-forming systems such as blue compact galaxies (BCDs or H II galaxies), and starburst systems. GEHRs in an individual galaxy are known to differ from one another in many of the observational properties, but still have several properties in common. The common properties such as the constancy of luminosity and diameter of the brightest (also largest) H II regions have been used earlier for estimating the distances to galaxies (Sandage & Tammann 1974, Kennicutt 1979). It is important to investigate the reasons for similarities as well as differences between different H II regions in order to make use of GEHRs as reliable distance indicators or tracers of star formation rates in galaxies.

Initial mass function (IMF), age, history, metallicity, extinction, mass or luminosity are among the most important parameters determining the properties of GEHRs. In recent years, there have been several attempts to investigate the IMF parameters under a variety of conditions (see Scalo 1986). Yet, the IMF slope of $\alpha=2.35$ as obtained by Salpeter (1955) remains the most accepted value. Humphreys & McElory (1984) have favoured a much steeper IMF for high mass stars in the Galaxy, while Parker & Garmany (1993) obtained an IMF slope close to Salpeter's value for the stars in 30 Doradus, both studies being based on star counts. Investigations based on the integrated properties of GEHRs have so far remained inconclusive on the exact value of IMF slope and the lower and upper cutoff masses. There are some indications that IMF may be flatter or deficient in low mass stars in active starburst regions (Scalo 1987).

In this study we aim to investigate the star formation histories of GEHRs, taking into account the possible IMF differences from one region to another. It is however important to take into account the effects of (i) interstellar extinction, (ii) metallicity and (iii) nebular contributions on the observable quantities, before these quantities can be compared with the synthetic models. Interstellar extinction is conventionally derived using the observed ratios of Balmer lines (see, e.g., Shields 1990). Balmer decrements as well as metallicities and nebular contributions can be derived from spectroscopic data on individual regions. With the above problems in mind, we use the BVRHα data of only those GEHRs from Mayya (1994) for which additional spectroscopy is available in the literature. The data, after applying corrections for extinction and nebular contribution, are compared with the evolutionary population synthesis model to investigate the properties of star formation in the sample regions. Analyses were performed on dimensionless diagrams, thus eliminating the possible errors due to the uncertainties in the estimation of distance to the source and/or the mass of the star-forming region. We find that the extinction experienced by the embedded cluster stars is lower compared to the values derived from the Balmer decrement. These results are of special in-

[1]Infra Red Astronomy Group, Tata Institute of Fundamental Research, Homi Bhabha Road, Colaba, Bombay 400 005, India.

 0004-6256/96/111(3)/1252/15/$6.00

terest, especially after a similar conclusion has been reached by the independent study of Calzetti *et al.*(1994) using ultraviolet (UV) and optical spectra of central regions of galaxies. Our study also reveals a slightly complex history of star formation in GEHRs.

In Sec. 2, we describe the sample and the method followed in extracting the pure stellar continuum from the observed *BVR* data. In Sec. 3, the properties of the embedded cluster are compared with population synthesis models. Our results are discussed in the context of recent results in Sec. 4. Physical models for star formation in GEHRs and the distribution of cluster stars, gas and dust are proposed in Sec. 5. Section 6 summarizes the main results of this study.

2. SOURCES OF DATA AND PRELIMINARY TREATMENT

The GEHR data for this study are taken from the *BVR*Hα photometric catalogue of Mayya (1994, Paper I henceforth). The catalogue contains CCD aperture photometric data on nearly 180 regions in nine nearby galaxies. In these studies, special care was taken in ensuring that the contamination by the background is minimum and hence the derived magnitudes are genuinely from the embedded cluster and the surrounding nebulosity. The usage of apertures rather than slits, as well as measurement of *BVR* continuum and Hα emission line fluxes, centered on the same pixel, makes these measurements ideally suited for the investigation of star formation properties. Spectroscopic data are available for about one fourth of these regions ($\sim$45). The sensitiveness of the background values on the catalogued colors is indicated by a photometric quality index in the catalogue. Regions having photometric quality index 4 (background uncertainties leading to errors in excess of 0.3 mag in $B-V$ and $V-R$ colors: see Appendix in Paper I for a discussion on background subtraction errors in H II region photometry) are dropped to eliminate background dominated regions from the sample. The estimated rms errors for the entire sample in the catalogue are <0.15 mag in colors and <0.05 dex in the ratio of Hβ to blue band luminosity (ϕ/L_B). The regions selected for the study here are relatively brighter and hence the errors are expected to be smaller. We estimate the errors to be a factor of two less as compared to that for the entire sample. Finally, we are left with 5 regions in NGC 1365, 3 in NGC 2903, 14 in NGC 2997, 2 in NGC 3351, 3 in NGC 4303 in addition to the giant H II complex NGC 2363 in NGC 2366 and the starburst nucleus of NGC 5253. Measurements using bigger apertures, which include more than one emitting knot, are also included around six regions in NGC 2997.

The spectroscopic data involving [O III] and Balmer lines are used to estimate the abundance of oxygen, electron temperature (T_e) and visual extinction (A_v(Bal)) using a semi-empirical approach (McCall *et al.* 1985). All the observed quantities have to be corrected for interstellar extinction before comparing with the models. Total extinction towards extragalactic H II regions consists of three parts—(i) extinction from the interstellar medium (ISM) of our galaxy (A_v(gal)), (ii) extinction from the ISM of the parent galaxy outside the H II region (A_v(ext)) and (iii) extinction due to the dust mixed with the gas within the H II region (A_v(int)). A_v(gal) values for the program galaxies are given in Table 1 for each of the program galaxies, as tabulated by de Vaucouleurs *et al.* (1991). Other quantities in the table are distances to the parent galaxies, number of regions used in the present study and the sources of spectroscopic data and distances. We denote the visual extinction as derived from the Balmer decrement by A_v, in the remaining part of the text, though it contains contribution from all the three components. We start our study using A_v to deredden the cluster and nebular quantities, assuming that the spectroscopically derived values are valid for both the cluster continuum and the nebular radiation integrated over the apertures. In the later part of this section, we suggest alternative prescriptions for extinction corrections that are necessary to explain the present data set.

TABLE 1. The sample of galaxies.

Galaxy NGC	deV. Type	A_v(gal)	Incl. (°)	Velocity km s^{-1}	Distance (Mpc)	Reference dist	Reference spect	$\mathcal{N}$(H II)
1365	SB(s)b	0.000	56	1502	10.0	1	8,9	5
2366	SBm	0.136	62	252	3.6	2	10,11	1
2903	SAB(rs)bc	0.053	58	467	10.0	3	12	3
2997	S(s)c	0.409	37	805	10.0	4	13,14	20
3351	SB(r)b	0.038	46	673	8.5	5	12	2
4303	SAB(rs)bc	0.000	24	1483	19.0	6	15	3
5253	Irr IIp	0.152	64	209	2.0	7	16	1

Quantities in columns 2, 3, 4 and 5 are from de Vaucouleurs *et al.* (1991) (RC3)

References for Table 1.

(1) Jones & Jones (1980); (2) Sandage & Tammann (1976); (3) Sandage & Tammann (1981); (4) Peterson (1978); (5) Bottinelli *et al.* (1984); (6) Kennicutt (1981); (7) de Vaucouleurs (1979); (8) Roy & Walsh (1988); (9) Alloin *et al.* (1981); (10) Peimbert *et al.* (1986); (11) Kennicutt *et al.* (1980); (12) McCall *el al.* (1985); (13) Walsh & Roy (1989b); (14) Roy & Walsh (1987); (15) Shields *et al.* (1991); (16) Walsh & Roy (1989a);

The usage of A_v to deredden quantities related to embedded clusters is appropriate only if the amount of dust residing internal to H II regions is negligible. The large spread in extinction values for regions within a single galaxy implies non-uniform distribution of dust within the parent galaxy, either within or outside the H II region. There have been studies investigating the relative contribution of the dust mixed with the ionized gas, known as "internal extinction," to the total extinction from the parent galaxy (Lequeux *et al.* 1981). These studies show the internal extinction to be non-negligible at least for some regions. The extinction values derived using the radio thermal continuum is statistically known to be higher than that derived using the Balmer decrement (Israel & Kennicutt 1980). Caplan & Deharveng (1986) have studied the effect of different dust configurations, including the dust internal to the H II regions to explain the observed discrepancy between the radio and optically derived extinction values. Internal reddening is found to be significant for some regions in the Large Magellanic Cloud (LMC). We find the extinction properties of embedded cluster stars to be different from that of the ionized gas and hence suggest an alternate prescription for extinction correction in GEHRs.

The Hα band fluxes have contribution also from [N II] lines at λ6548, 6583 Å . The observed Hα+[N II] fluxes are

first corrected for interstellar extinction using A_v and the galactic extinction curve (Seaton 1979). Hα fluxes are computed from the observed Hα+[N II] fluxes using the spectroscopically determined [N II]/Hα ratios. Lyman continuum luminosities are derived from extinction corrected Hα luminosities using

$$\frac{N_L}{\text{phs}^{-1}} = 7.32\times 10^{11}\frac{\text{H}\alpha}{\text{erg s}^{-1}} \quad (1)$$

which assumes an ionization bounded case B nebula (Osterbrock 1989). The expected Hβ luminosity (ϕ) is computed from this using

$$\frac{\phi}{\text{erg s}^{-1}} = 4.78\times 10^{-13}\frac{N_L}{\text{phs}^{-1}}. \quad (2)$$

The treatment of broad-band magnitudes is slightly different. First, an estimation of the contribution from the nebula (line +continuum) within each band is made based on the derived T_e and extinction corrected Hα luminosity. The strengths of all bright lines relative to Hβ line, are taken from McCall *et al.* (1985). Free-free, free-bound and 2-photon emission mechanisms are considered in computing the nebular continuum. Details of these computations are presented in Mayya (1995). For a majority of the regions, the nebular corrections amount to $<5\%$ in B and V bands and 15–25% in the R band, with emission lines being the main contributors. The estimated nebular contributions to B and V bands exceed that in the R band in the two high excitation regions (NGC 2363 and 5253), due to the presence of strong [O III] lines. However, these estimates heavily depend on the assumed shape of the passband, because of the location of the [O III] lines in the steeply falling part of the B and V band responses. We find that even a 50 Å shift of the V band response curve to longer wavelengths changes the $B-V$ and $V-R$ colors by as much as 0.3 mag in NGC 2363. This amount of shift of the effective wavelength is not unusual and hence gaseous corrected cluster colors using broad bands are bound to have large errors for high excitation regions. Use of narrower bands situated at emission line free regions would have eliminated this source of uncertainty.

The estimated nebular luminosities are subtracted from extinction corrected broad band luminosities to obtain pure cluster quantities. These quantities are reddened back to obtain the observationally expected values without any contamination from the surrounding nebula. We denote these quantities by the subscript *, while the observed quantities are denoted by the subscript "obs" (e.g., $(B_{\text{obs}}, (B-V)_*$ etc.). The resultant quantities are corrected for the galactic and total extinction using A_v(gal) and A_v and are denoted by suffixes 1 and 2 respectively. The Galactic extinction curve as tabulated by Seaton (1979) is used in these computations. The process is summarized below.

$$(B-V)_{\text{obs}} - \text{gas subt} \rightarrow (\text{B-V})_*, \quad (3)$$

$$(B-V)_* - \text{A}_\text{v}(\text{ gal}) \rightarrow (\text{B-V})_1, \quad (4)$$

$$(B-V)_* - \text{A}_\text{v}(\text{ Bal}) \rightarrow (\text{B-V})_2. \quad (5)$$

Table 2 contains the results for individual H II regions. Column 1 contains identification numbers for GEHRs following Paper I. Oxygen abundances in column 2 are derived from $(I[\text{O II}]+I[\text{O III}])/I(\text{H}\beta)$ ratio using the semi-empirical calibration of McCall *et al.* (1985). Note that the sample regions have metallicities in the range $2-4Z_\odot$, with the exception of the two high excitation regions mentioned above. McCall *et al.* also provide relation between the oxygen abundance and T_e, which is used to derive T_e given in column 3. Column 4 lists the visual extinction based on the Balmer decrement. Oxygen abundance and visual extinction are based on the sources of spectroscopic data listed in Table 1. While deriving the visual extinction, the underlying absorption in Balmer lines, which at the most contributes about 2 Å in Hβ equivalent width (McCall *et al.* 1985), has been accounted for. The V_* magnitude, and $(B-V)_*$ and $(V-R)_*$ colors in columns 5, 6 and 7 respectively, are cluster quantities after subtracting the gaseous contribution. Column 8 contains the $\log(\phi/L_B)_* = \log(\phi)-\log(L_B)_*$ values. Note that A_v(Bal) has been used in obtaining the extinction corrected ϕ from observations. Lyman continuum luminosity is given in column 13. Remaining columns in the table will be explained in the next section.

3. COMPARISON WITH MODELS

We plot in Fig. 1 the values of $\log(\phi/L_B)_1$ against $(B-V)_1$, which are corrected only for galactic extinction. Figure 2 shows a similar plot, but with $(V-R)_1$ replacing $(B-V)_1$. H II regions from different galaxies are shown by different symbols, as indicated at the right hand side of the diagram. The small and large aperture measurements are distinguished in the case of NGC 2997. Rms errors on the plotted quantities are indicated by the cross at the bottom-left corner of the diagram. For the two high excitation regions, NGC 2363 and 5253, there is an additional source of error, arising out of the subtraction of nebular contribution, as discussed in the previous section. The arrow on the right side of the figure is the reddening vector, with its length corresponding to 1 magnitude of visual extinction.

The observed quantities are compared with the evolutionary population model, which is briefly described below. The computational details and results for different star formation scenarios can be found in Mayya (1995: Paper II henceforth). The evolutionary population synthesis model is based on the input stellar evolutionary data of Schaller *et al.* (1992), and stellar atmosphere data of Kurucz (1992). The cluster is defined by an initial mass function, age, metallicity and the total mass in stars. The evolution of the cluster is performed at every 0.1 Myr interval, which is adequate to sample even the fast evolutionary phases of massive stars. Optical and near infrared colors are computed and tabulated in Paper II for three different scenarios of star formation at solar metallicity. As noted earlier, GEHRs in the present sample have metallicities between $2-4Z_\odot$, with the exception of NGC 2363 and 5253 ($\frac{1}{5}$ and $\frac{1}{3}Z_\odot$ respectively). Recently, Cerviño & Mas-Hesse (1994) and Leitherer & Heckman (1995), have shown the metallicity differences to affect the cluster evolution significantly. Hence we extended the model computations of Paper II to $Z=0.1Z_\odot$ and $Z=2Z_\odot$ based on the stellar evolutionary tracks of Schaller *et al.* (1992) and

TABLE 2. Derived properties of GEHRs.

Ident	12+ log($\frac{O}{H}$)	T_e K	A_v	V_*	$(B-V)_*$	$(V-R)_*$	$\left(\frac{\phi}{L_B}\right)_*$†	A_{vc}	$(B-V)_3$	$(V-R)_3$	$\left(\frac{\phi}{L_B}\right)_3$†	N_L† ph s^{-1}	M_T† $M_\odot$
N1365-1	9.13	6000	0.91	16.79	0.17	−0.02	−1.24	0.45	0.02	−0.13	−1.48	51.15	5.25
N1365-2	9.20	5626	1.07	15.80	0.16	0.14	−1.15	0.53	−0.01	0.00	−1.43	51.63	5.73
N1365-3	9.11	6083	0.86	16.99	0.24	0.06	−1.18	0.43	0.10	−0.05	−1.40	51.10	5.20
N1365-4	9.20	5627	1.10	16.34	0.24	0.14	−1.35	0.55	0.06	−0.00	−1.64	51.19	5.29
N1365-5	9.13	6014	0.96	16.25	0.34	0.13	−1.70	0.48	0.19	0.01	−1.95	50.83	5.53
N2363	8.06	12180	0.45	14.74	−0.22	0.52	−0.68	0.29	−0.31	0.45	−0.83	51.96	5.56
N2903-1	9.29	5153	1.97	17.35	0.37	0.66	−0.40	1.01	0.05	0.40	−0.92	51.68	5.28
N2903-2	9.26	5317	0.29	16.77	0.01	0.34	−1.23	0.17	−0.04	0.30	−1.32	51.23	4.83
N2903-13	9.37	4671	2.39	16.75	0.15	0.54	−0.33	1.22	−0.24	0.23	−0.97	51.23	4.83
N2997NE-1	9.18	5726	2.13	17.55	0.25	0.60	−0.40	1.27	−0.15	0.28	−1.06	51.65	5.25
N2997NE-2	9.29	5129	1.58	18.10	0.23	0.18	−0.84	1.00	−0.09	−0.07	−1.35	51.00	4.60
N2997NE-7	9.25	5369	1.90	18.76	0.11	0.22	−0.96	1.16	−0.26	−0.07	−1.57	50.66	4.26
N2997NE-9	9.29	5124	1.30	19.13	0.10	0.35	−0.99	0.85	−0.18	0.13	−1.43	50.66	4.76
N2997NE-10	9.32	5000	1.33	17.47	0.07	0.18	−1.23	0.87	−0.21	−0.04	−1.68	50.93	5.03
N2997NE-12	9.30	5100	1.60	18.50	0.18	0.26	−0.89	1.01	−0.14	0.01	−1.42	50.80	4.90
N2997NE-13	9.22	5510	1.81	18.90	0.08	0.12	−1.08	1.11	−0.27	−0.16	−1.65	50.50	4.10
N2997NE-14	9.22	5510	1.81	19.14	0.19	0.30	−1.30	1.11	−0.17	0.02	−1.87	50.14	4.24
N2997NE-15	9.22	5510	1.81	19.56	0.49	0.27	−0.38	1.11	0.14	−0.01	−0.95	50.66	4.26
N2997NE-24	9.17	5771	1.40	18.19	0.16	0.15	−1.31	0.90	−0.13	−0.07	−1.78	50.52	4.62
N2997NE-34	9.21	5537	2.43	17.67	0.31	0.46	−0.82	1.42	−0.14	0.11	−1.56	51.16	5.26
N2997SW-1	9.34	4821	1.63	17.27	0.53	0.50	−0.94	1.02	0.20	0.25	−1.47	51.11	5.21
N2997SW-2	9.29	5136	2.15	17.32	0.38	0.44	−0.37	1.28	−0.03	0.12	−1.04	51.71	5.31
N2997SW-3	9.30	5084	2.04	16.37	0.33	0.40	−0.90	1.23	−0.06	0.09	−1.54	51.59	5.69
N3351-1	9.50	3921	1.75	17.60	−0.05	0.30	−1.26	0.89	−0.33	0.08	−1.72	50.74	4.34
N3351-2	9.42	4374	1.97	14.62	0.55	0.58	−1.26	1.00	0.23	0.33	−1.78	51.65	5.75
N4303-4	9.21	5526	0.43	15.96	0.20	0.31	−1.20	0.22	0.13	0.25	−1.31	52.06	5.66
N4303-9	9.35	4795	0.86	16.50	0.25	0.34	−1.29	0.43	0.11	0.24	−1.51	51.74	5.84
N4303-24	9.33	4927	0.43	16.50	0.20	0.25	−1.53	0.22	0.13	0.20	−1.64	51.52	5.62
N5253-1	8.37	10410	0.95	13.77	0.18	0.35	−0.70	0.55	0.00	0.21	−0.98	51.56	5.16
N2997NE-G1	9.19	5637	2.24	15.76	0.36	0.32	−0.50	1.32	−0.06	−0.01	−1.19	52.22	5.82
N2997NE-G2	9.25	5362	2.00	17.00	0.06	0.42	−0.85	1.21	−0.33	0.12	−1.48	51.50	5.60
N2997NE-G3	9.30	5090	1.38	18.08	0.19	0.28	−0.97	0.89	−0.10	0.06	−1.44	50.89	4.99
N2997NE-G4	9.31	5033	1.81	17.57	0.16	0.51	−0.52	1.11	−0.20	0.24	−1.10	51.55	5.15
N2997NE-G5	9.19	5650	2.09	17.75	0.28	0.19	−0.46	1.25	−0.12	−0.12	−1.11	51.49	5.09
N2997NE-G8	9.21	5537	2.43	16.50	0.18	0.56	−0.94	1.42	−0.27	0.21	−1.67	51.56	5.66

†in log units

Schaerer *et al.* (1993), respectively. Metal-poor models are particularly important for the study the star formation in blue compact galaxies. Note that the metallicity of the most metal-poor galaxy, I Zw 18 is around a factor of 4 smaller than our metal-poor model. The evolutionary tracks for an instantaneous burst (IB) of star formation at the three metallicities are shown in Figs. 1 and 2. The long-dashed curve represents the solar metallicity model, while the short-dashed and the solid curves represent $0.1Z_\odot$ and $2Z_\odot$ models respectively. The clusters are evolved upto 6.5 Myr, with dots placed on the curves at every 0.5 Myr. The evolutionary phase corresponding to 4 Myr is indicated by the letter 4 on each of the curves. The IMF chosen is close to Salpeter's: $m_l = 1\ M_\odot$, $m_u = 60\ M_\odot$ and $\alpha = 2.5$.

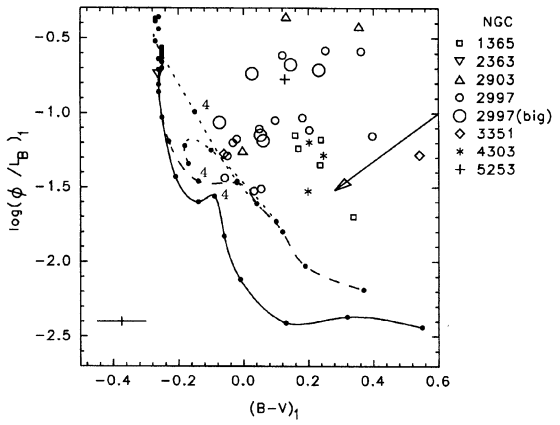

FIG. 1. Observed GEHRs in $\log(\phi/L_B)_1$ vs $(B-V)_1$ plane. The nebular contribution is subtracted from broad bands and extinction corrections are done only for galactic dust. Typical rms errors are shown by the cross at the bottom left corner. The arrow indicates extinction correction corresponding to $A_v = 1$ mag. The evolution of clusters at $Z = 0.1,1$ and $2Z_\odot$ are shown by the short-dashed, long-dashed and solid curves respectively. An IMF with parameters $m_u = 60$ and $\alpha = 2.5$ is used. The dots on the line are spaced 0.5 Myr apart with the dot corresponding to 4 Myr marked by the letter 4.

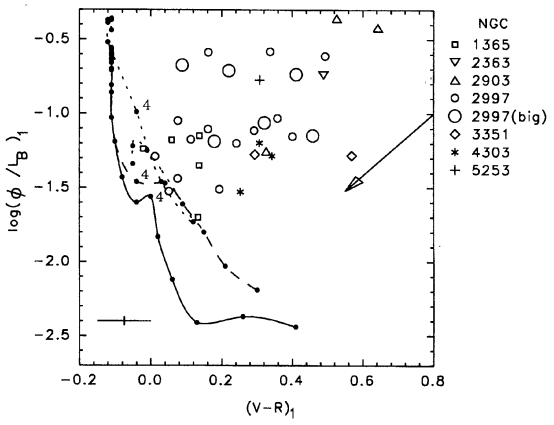

FIG. 2. Observed regions in $\log(\phi/L_B)_1$ vs $(V-R)_1$ plane. See Fig. 1 for other details.

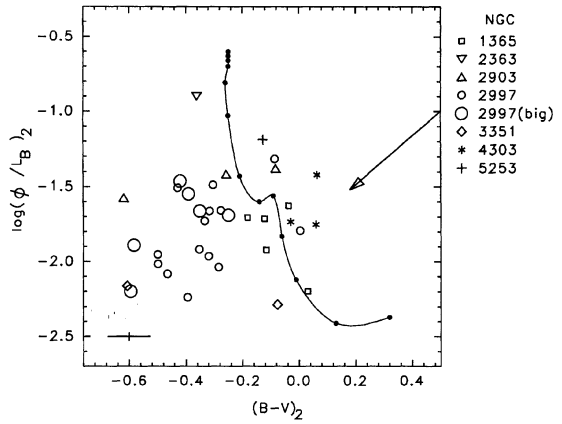

FIG. 3. Observed regions in $\log(\phi/L_B)_2$ vs $(B-V)_2$ plane. Extinction corrections are done based on the Balmer decrement. Other details are as in Fig. 1, except that only $Z=2Z_\odot$ model is shown and the evolution is shown only upto 6 Myr.

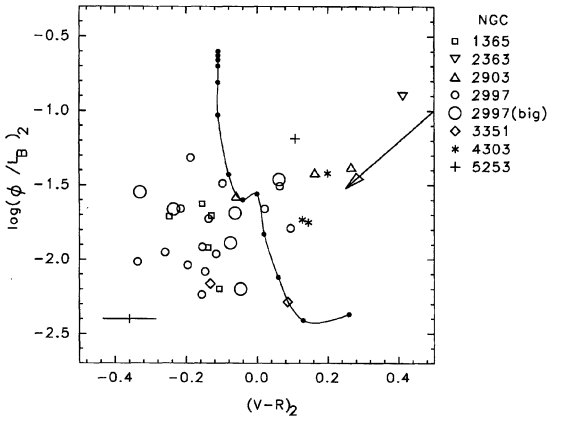

FIG. 4. Observed regions in $\log(\phi/L_B)_2$ vs $(V-R)_2$ plane. See Fig. 3 for other details.

Two phases can be distinguished during the early (age <10 Myr) evolution of an IB. The first phase is controlled by the massive main sequence stars while the second by the supergiants, in particular the red supergiants. The transition from the first phase to second phase takes place around 4–5 Myr, with metallicity playing a major role during both the phases. The main sequence lifetime of the stars decreases with the increasing metallicity resulting in a faster drop of ϕ/L_B in metal-rich regions during the first phase. Higher metallicity favours the formation of red supergiants (RSGs) and Wolf-Rayet stars in the cluster and hence a given burst of star formation produces more of these stars in a metal-rich environment. Additionally the metal-rich RSGs are cooler than the metal-poor RSGs, resulting in redder colors during the red supergiant phase of metal-rich clusters. The increased optical luminosity due to RSGs in metal-rich regions also leads to a decrease of ϕ/L_B. The metal-poor locus turns back at 5 Myr (ϕ/L_B increases and colors become bluer), which can be understood in terms of the absence of long lived cooler supergiants in the cluster. Thus, the metal-rich clusters have lower values of ϕ/L_B throughout their evolution, and redder colors after around 4 Myr of evolution in comparison to metal-poor regions. A majority of the regions in our GEHR sample are metal rich and hence we use $Z=2Z_\odot$ models for comparison with our data.

For m_u other than 60 (stellar masses are expressed in solar units henceforth) the evolutionary track is similar to the one shown, except that the starting (age = 0) ϕ/L_B value is different. For $m_u>60$, it starts at a higher value than shown and the converse is true for lower masses. At $\alpha=2.5$, the $B-V$ color reddens by 0.04 mag as the upper cutoff is decreased from 120 to $30M_\odot$, whereas $\log(\phi/L_B)$ decreases by 0.70 dex for the same range of masses. As the more massive stars die, the evolution follows that of a cluster with a lower m_u.

It can be noticed that the evolutionary track forms an envelope around the observed points. All the observed points can be brought into the locus expected from the $Z=2Z_\odot$ model, by shifting the points along the reddening vector by amounts $A_v=0$–1.4 mag. The giant H II complex NGC 2363 has several properties which distinguishes it from the rest of the sample, and hence we treat this region separately in the discussions to follow. The distinguishing properties are its low metallicity, negligible extinction (Kennicutt *et al.* 1980), and a large correction for the nebular contribution in B,V and R bands.

In Figs. 3 and 4, the observed quantities are plotted after dereddening by A_v, as derived from Balmer decrement (quantities with suffix 2). Other details in these figures are similar to Figs. 1 and 2, except that only $Z=2Z_\odot$ evolutionary track is shown and the track is truncated at 6 Myr instead of 6.5 Myr. It is striking to note that the reddening correction has moved the points away from the models in both the axes. Hence the corrected $B-V$ and $V-R$ colors are too blue and (ϕ/L_B) too low compared to the values expected for clusters younger than around 4 Myr. One can infer from Figs. 1 and 2, that there are many regions for which very little extinction correction is required, whereas the extinction values computed using the Balmer decrement have a median value close to 1.5 mag, with only 4 regions having values less than 0.75 mag. These two figures indicate that by dereddening the cluster related quantities by extinction derived from the Balmer decrement, we are over-correcting for extinction. In order to investigate this in more detail, we plot in Fig. 5, the dereddened $(B-V)_2$ colors against the pure extra-galactic visual extinction $A_v-A_v(\mathrm{gal})$. A trend of blue $(B-V)_2$ colors having higher extinction is clearly seen in the figure. A similar trend is also seen in $(V-R)_2$ color, but to a lesser degree (not plotted). In fact both $(B-V)_2$ and $(V-R)_2$ colors are bluer than the model for regions having $A_v>1.5$ mag. The figure gives an important clue on the nature of interstellar extinction towards stellar continuum and ionized gas emission in GEHRs. The inescapable conclusion from Figs. 3, 4 and 5 is that the cluster continuum on an average experiences lesser extinction than the emission from the ionized gas. Such a situation is possible if most of the extragalactic extinction is due to the dust internal to GEHRs and the radiation from the ionized gas is selectively absorbed by the dust. The ionized gas in GEHRs is known to be confined to

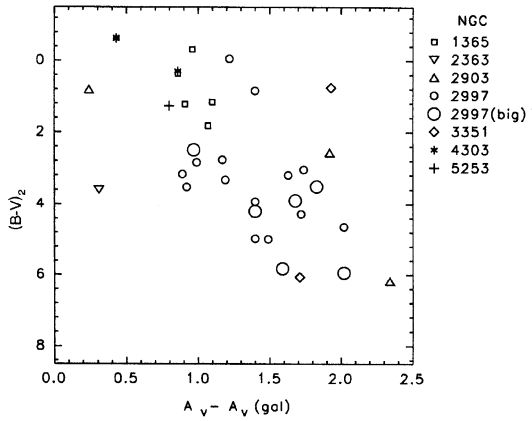

FIG. 5. The $B-V$ colors after correction for extinction derived from the Balmer decrement are plotted against A_v corrected for galactic extinction. Note the trend of bluer regions having larger A_v.

clumps, with a volume filling factor as small as 0.01 (Shields 1990). The dust is also likely to be present in the same volume. Radiation from the stars, which contribute to the optical and UV continuum, on the other hand might occupy less dustier regions, and hence experience lesser amount of extinction. The segregation might be arising as a result of relative motion of the stars with respect to the gaseous material from which they have formed (Leisawitz & Hauser 1988). Based on this simple clumpy model, we formulate a different prescription to estimate the extinction of the stellar continuum which should be more accurate at least statistically.

3.1 Estimation of Extinction towards Cluster Continuum

The observed range of colors is too large to be explained in terms of IMF variations. For an assumed slope of the IMF, the $B-V$ color reddens by ≤ 0.04 mag as m_u decreases from 120 to $30M_\odot$. Color differences are around 0.20 mag even for two extreme IMFs, one rich in massive stars ($m_u=120$, $\alpha=1.0$), and the other rich in low mass stars ($m_u=30$, $\alpha=3.5$). Thus, as a first approximation, we can neglect the dependence of colors on the IMF for clusters younger than 3.5 Myr. We assume $B-V=-0.25$ and $V-R=-0.10$ as typical values for the young clusters in our sample, corresponding to $\alpha=2.5$ and $Z=2Z_\odot$. The remaining part of the discussion pertains to the IMF parameters $m_l=1$, $m_u=60$, $\alpha=2.5$, unless otherwise mentioned. The regions having high ϕ/L_B value in addition to blue $B-V$ and $V-R$ colors must be the youngest regions in the sample. We hence make independent estimate of visual extinction (A_{vc}) towards stellar continuum on the basis that dereddened $B-V$ and $V-R$ colors cannot be bluer than -0.25 and -0.10 respectively. The method is summarized by the following equations, which are based on the formulation of Calzetti *et al.* (1994).

Consider an embedded cluster with intrinsic intensity I_λ^0 at a given wavelength. The intensity I_λ leaving the parent galaxy is then given by,

$$I_\lambda = I_\lambda^0 \exp(-\tau_\lambda), \tag{6}$$

where τ_λ is the line of sight optical depth suffered by the radiation at wavelength λ in the host galaxy. If τ_β and τ_α are the optical depths experienced by the Balmer line photons Hβ and Hα respectively, then the differential optical depth between Hβ and Hα is given by,

$$\tau_B^l = \tau_\beta - \tau_\alpha = \ln\left(\frac{(H\alpha/H\beta)_i}{2.86}\right), \tag{7}$$

where $(H\alpha/H\beta)_i$ is the ratio of intensities of Hα and Hβ lines after correcting for galactic extinction. Visual extinction A_v tabulated in Table 2 is related to τ_B^l by,

$$A_v(\text{ Bal}) - A_v(\text{ gal}) = \frac{1.086\times 3.1}{X_\beta - X_\alpha}\,\tau_B^l, \tag{8}$$

or

$$\tau_B^l = 0.354(A_v(\text{ Bal}) - A_v(\text{ gal}))\,, \tag{9}$$

where X_β and X_α are tabulated by Seaton (1979) for the galactic extinction curve. τ_B^l as defined above is the difference in extinction between Hβ and Hα emission lines. Analogously we can define the extinction suffered by the continuum photons between Hβ and Hα wavelengths. We denote this quantity as τ_B^c defined as,

$$\tau_B^c = \tau_\beta^c - \tau_\alpha^c = \frac{X_\beta - X_\alpha}{1.086} E(B-V)_i\,, \tag{10}$$

where

$$E(B-V)_i = (B-V)_{\rm obs} - (B-V)_{\rm mod} - A_v(\text{ gal})/3.1. \tag{11}$$

We define,

$$g = \frac{\tau_B^c}{\tau_B^l} = \frac{A_{vc} - A_v(\text{ gal})}{A_v - A_v(\text{ gal})}. \tag{12}$$

Equations similar to the above are also formulated for the determination of g from the observed $V-R$ colors. There are 11 regions in the sample for which both $(B-V)_2$ and $(V-R)_2$ are bluer than the bluest model colors. We derive a mean value of $g=0.70\pm0.20$, from both these colors. Physically g is controlled by the spatial distribution of gas, dust and stars with a value of unity if all the three components are well mixed inside the volume of GEHR or the entire dust is situated far away from the emitting region. However there are several issues which come in the way of an accurate determination of g, some of which are intrinsic to the region of interest and hence unavoidable, while others are due to observational errors on colors. In estimating g, we assumed all regions whose dereddened colors become bluer than the bluest model colors to be young. However a moderately evolved region with a lower value of g than estimated is indistinguishable from a young region with g value closer to unity. Thus the actual value of g could be smaller than the estimated mean. In estimating g, we also assumed that the entire extra-galactic extinction comes from within the star-forming complex. In reality, there may be some contribution from the ISM of the parent galaxy. Correction to this has the effect of decreasing the value of g. With all these considerations, we assume $g=0.50$ to be typical for the whole sample of GEHRs in the subsequent analysis. This value is sup-

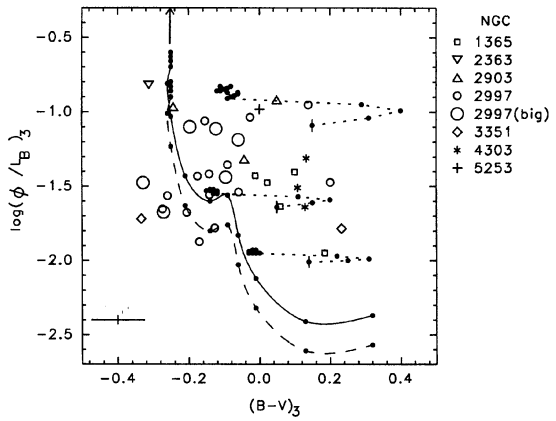

FIG. 6. Observed regions in $\log(\phi/L_B)_3$ vs $(B-V)_3$ plane. Extinction corrections are done using A_{vc} with $g=0.50$. Solid line represents the $Z=2Z_\odot$ model evolved upto 6 Myr. The same model is shifted by 0.20 dex (see text for details) and shown by the dashed line. A model with $m_u=120$ and no shift begins at the tip of the arrow. Sequences with short-dashed lines correspond to composite models with the younger population at 0 (top), 3 (middle) and 4.5 (bottom) Myr age superposed on an older population. The older population is 6–14 Myr old along the sequence. Each sequence begins with a dot marked by vertical line.

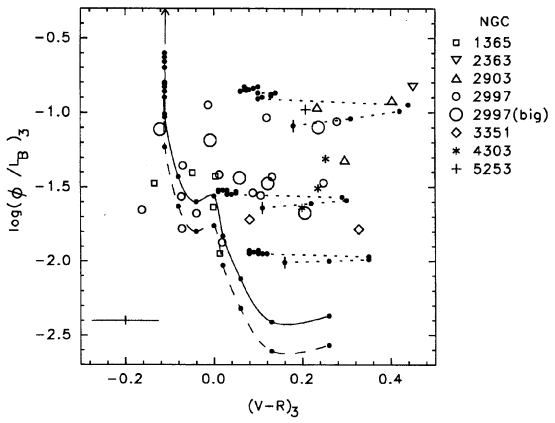

FIG. 7. Observed regions in $\log(\phi/L_B)_3$ vs $(V-R)_3$ plane. See Fig. 6 for other details.

ported by a recent analysis involving UV continuum and Balmer lines of central regions of galaxies (Calzetti *et al.* 1994). Using this average value, A_{vc} is recomputed for all the regions using Eq. 12. The resultant values are tabulated in column 9 of Table 2. The cluster quantities are dereddened using these values of A_{vc} and the resulting quantities are identified by suffix 3. Nebular quantities and hence ϕ are corrected for extinction using A_v.

$$(B-V)_* - \mathrm{A_{vc}} \rightarrow (\mathrm{B-V})_3. \tag{13}$$

The resultant values of $(\phi/L_B)_3$, $(B-V)_3$ and $(V-R)_3$ are tabulated in Table 2. $\log(\phi/L_B)_3$ is plotted against $(B-V)_3$ and $(V-R)_3$ in Figs. 6 and 7, respectively. As in the earlier figures the IB model for the chosen IMF is shown with solid curve, with dots placed every 0.5 Myr. The reddest point on the curve corresponds to 6 Myr of evolution. With the new prescription for extinction correction, not only the colors, but also the $\log(\phi/L_B)$ values are brought closer to the curve represented by the IB model. While a set of regions follow this track in both the diagrams within the observational errors, there are some regions which lie below and some others which lie to the right (redward) of the solid line. These regions require alternative models, which is the main theme of the discussion in the remaining part of this section.

3.2. *Destruction and Escape of Ionizing Photons*

There are statistically significant number of regions which have blue colors, indicative of young age, but have ϕ/L_Bvalues lower than that expected for a cluster younger than 3 Myr. These regions seem to agree well with the model, if the $\log(\phi/L_B)$ is shifted by about -0.2 dex, as indicated by the dashed curve in Figs. 6 and 7. The possible sources, which can give rise to this shift are investigated below. We express the discrepancy in $\log(\phi/L_B)$ between observations and the model evolutionary track by a parameter f defined as,

$$\log\left(\frac{\phi}{L_B}\right)_{\mathrm{obs}} = \log\left(\frac{\phi}{L_B}\right)_{\mathrm{mod}}(t) + \log f, \tag{14}$$

where $(\phi/L_B)_{\mathrm{obs}}=(\phi/L_B)_3$ and $\log(\phi/L_B)_{\mathrm{mod}}(t)$ is the IB model value at age t. For the IB model, changes in ϕ/L_B are mainly controlled by the changes in ϕ and hence, physically, f is the ratio of the detectable number of Lyman continuum photons to that expected from the model and has a maximum value of 1 when every Lyman continuum photon emitted by the cluster stars at the estimated age can be traced by the Balmer emission lines. We estimate ages between 2.5–4 Myr for the regions which require -0.2 dex shift. This value of shift implies a value of $f=0.65$ or 35% of the ionizing photons could not be traced by the Hα emission.

The following processes may be responsible for the missing ionizing photons: (i) the destruction of ionizing photons by dust within the ionized complexes (η_{dust}), and (ii) the escape of ionizing photons from the nebula or an underestimation of Hα flux, which traces the ionizing photon rate (η_{esc}). The under-estimation may be caused by the total absorption of Hα photons by dust clumps or because a significant fraction of the total Hα luminosity is in low surface brightness halo component, which lies below the detection limit in most cases. η_{dust} and η_{esc} are related to f by the eq.,

$$f=(1-\eta_{\mathrm{dust}})(1-\eta_{\mathrm{esc}}). \tag{15}$$

Good estimates of η_{dust}, η_{esc} are lacking both observationally and theoretically. Smith *et al.* (1978) and Mezger (1978) have estimated η_{dust} to be between 0.7 and 0.2 for giant galactic H II regions. Belfort *et al.* (1987) have assumed a useful mean value of $\eta_{\mathrm{dust}}=0.30$, a value also used by many others (see, e.g., Mas-Hesse & Kunth 1991). The observed value of $f=0.65$, then corresponds to negligible η_{esc}. The value of f, however, depends on the assumed IMF parameters with the dependence weakening beyond 3 Myr.

From these analyses, it may be concluded that the absorption of ionizing photons by dust is the main source of the discrepancy in ϕ/L_B (or Balmer line equivalent widths) ob-

served in some regions, for the assumed IMF parameters. This is also supported by our conclusion based on cluster colors, that dust resides inside GEHRs. On the other hand a non-zero η_{esc} cannot be completely ruled out because of the uncertainties in m_u, age and absorption fraction of ionizing photons by dust. The detection of extra-H II region ionized gas in several irregular galaxies by Hunter & Gallagher (1992) and Hunter *et al.* (1993) has raised questions regarding the source of ionization of these diffuse regions. The Lyman continuum photons escaping the H II complexes may explain the observed ionization.

3.3. *Effect of Multiple Star Bursts*

The evolution of an instantaneous starburst with around 35% loss of the Lyman continuum photons, along with reduced effective extinction towards radiation from stars compared to that from the ionized gas, is found to explain the blueward envelope (within the limits of observational scatter) of regions in the $\log(\phi/L_B)$ vs $(B-V)$ and $(V-R)$ diagram. However, there is considerable spread of colors at any given ϕ/L_B which cannot be explained by an instantaneous burst model.

The departure of the colors from the IB model is in the redder direction, which can be understood in terms of a population rich in red supergiants, co-existing with the younger population. The two populations of different ages are seen spatially resolved in 30 Doradus (McGregor & Hyland 1981). The younger population provides the ionizing radiation whereas the red supergiant population contributes bulk of the optical continua. Stars in the mass range $40-15M_\odot$ become red supergiants at ages 4–14 Myr at $Z=2Z_\odot$ (Schaerer *et al.* 1993). Simultaneous existence of ionizing stars as well as red supergiants implies extended duration of star formation either proceeding continuously or in the form of bursts of short durations. The range of computed quantities for continuous star formation is small compared to the range of observed quantities (Paper II), and hence the continuous star formation cannot explain present observations. On the other hand, 2-burst models of Paper II reproduce much wider range of observable values. We discuss these models in order to explain our observations.

The composite model of two starbursts of equal strength with the younger one at 0, 3 and 4.5 Myr is shown in Figs. 6 and 7 as three sequences of short-dashed lines. Both the bursts assume IMF slope of 2.5 and $m_u=60$ and $Z=2Z_\odot$. In each of these sequences, the age of the older burst changes from 6–14 Myr, with beginnings of the sequences marked by the short vertical line followed by successive solid dots spaced every 0.5 Myr. The color for IB model becomes reddest at around 7 Myr corresponding to the RSG phase of stars around $25M_\odot$ mass, turning blue again at later stages of evolution. This is the cause of the blue-ward turnover of the 2-burst models. The general trend of many observed regions lying redward of the IB model is well reproduced by the 2-burst models, with younger burst ages between 0 and 4.5 Myr and the older burst in the supergiant-rich phase (age ~ 10 Myr).

For the regions with two bursts of star formation, the observed values of $\log(\phi/L_B)$ can be reproduced by models without the need for any process that significantly destroys the ionizing photons, unless the upper cut-off mass of IMF is higher than $60M_\odot$. In Figs. 6 and 7, the tip of the vertical arrow indicates the position of IB model at $t=0$ if m_u is increased to $120M_\odot$.

TABLE 3. Star formation histories of GEHRs.

IB ($t<3$ Myr)	IB ($t\sim3$–5 Myr)	2-burst ($t_{young}<3$ Myr)	2-burst ($t_{young}\sim3$–5 Myr)
N2363:	N2997NE-13	N1365-1:	N1365-5
N2997NE-2:	N2997NE-14	N1365-2	N3351-2
N2997NE-7:	N2997NE-24	N1365-3	
N2997NE-10	N2997SW-3:	N1365-4	
	N3351-1:	N2903-1	
		N2903-2	
		N2903-13:	
		N2997NE-1	
		N2997NE-9	
		N2997NE-12	
		N2997NE-15	
		N2997NE-34	
		N2997SW-1	
		N2997SW-2	
		N4303-4	
		N4303-9	
		N4303-24	
		N5253-1	
		N2997NE-G1	
		N2997NE-G2:	
		N2997NE-G3	
		N2997NE-G4	
		N2997NE-G5:	
		N2997NE-G8:	
14%	17%	62%	7%

3.4. *Classification of Sample GEHRs*

Based on the position of the GEHRs in $\log(\phi/L_B)_3$ vs $(B-V)_3$ and $(V-R)_3$ diagrams we classify the GEHRs into 5 groups. The classification is uncertain for those few regions with a poor correspondence between $B-V$ and $V-R$ colors. Nevertheless the classification is expected to throw more light on the evolutionary history of GEHRs in general. A short description of the five groups are given below.

1. Young regions ($t_{young}<3$ Myr) with instantaneous burst of star formation.

2. Moderately evolved regions ($t_{young}\sim$ 3–5 Myr) with instantaneous burst of star formation.

3. Young regions ($t<3$ Myr) with a co-existing population of red supergiants from a previous generation.

4. Moderately evolved regions ($t_{young}\sim3$–5 Myr) with a co-existing population of red supergiants from a previous generation.

5. Evolved regions ($t>5$ Myr) rich in red supergiants containing stars from one or two bursts.

Table 3 lists the objects classified under each group. None of the regions in our sample can be classified into group 5. The last row in the table gives the percentage of observed regions in each group. A colon in front of an entry suggests that the classification is uncertain either because of lack of correspondence between $B-V$ and $V-R$ colors or due to more than one model occupying a given region in our diag-

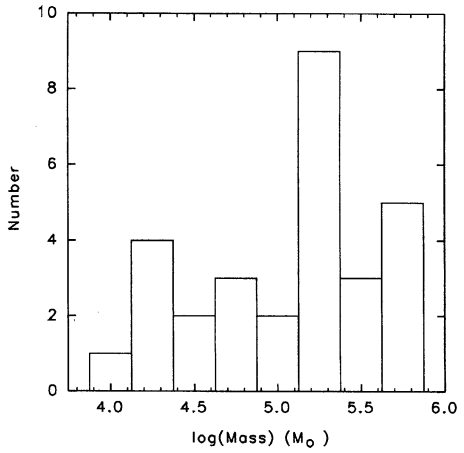

FIG. 8. Histogram of masses of GEHRs.

nostic diagrams (within the observational errors). The classification helps us to draw the following conclusions.

1. Seventy percent of the sample regions contain stars from more than one burst over the last 10 Myr. The most recent burst has occurred within the last 3 Myr in 90% of these regions.

2. The frequency of detection of young single burst regions is low, implying that the first generation of stars might be occurring deep inside the clouds, and hence are optically obscured when they are young and luminous.

A detailed scenario of star formation, incorporating all the observed properties is proposed in section 5.

3.5. Masses of Embedded Clusters

For an assumed IMF, the mass of the star-forming complexes can be estimated based on the observed Lyman continuum luminosity of the regions. Corrections for the decrease in ionizing luminosity due to evolution, destruction by dust and possible escape of photons have to be made in order to obtain the total ionizing luminosity emitted from the cluster. The total mass (M_T) is thus given by,

$$\log(M_T) = \log(\phi)_{\rm obs} - \log f - \log(\phi)_{\rm mod}(t), \qquad (16)$$

where $(\phi)_{\rm mod}(t)$ is the ionizing luminosity per unit mass of the cluster at an age t, as derived from the model for an assumed IMF. The factor f takes care of the loss of ionizing photons with an estimated value between 0.65 and 1.0. A mean $(\phi)_{\rm mod}(t)$ is assigned for each group (Table 3), which is used in deriving the mass of individual regions. We further assumed that only the younger burst contributes ionizing luminosity, when two populations co-exist. The masses derived with these assumptions and an IMF with $\alpha = 2.5$ and $m_u = 60$ are given in the last column of Table 2. Their histogram distribution is given in Fig. 8 with a mean value of

$$\log(M_T) = 5.1 \pm 0.5$$

for the entire sample ($n = 29$). While estimating the masses we assumed $f = 1$, implying complete detection of ionizing photons. Depending on the exact value of f for a given region, the actual masses might be higher by a factor of up to 2. The above estimates indicate that the mean mass of a cluster is $\sim 10^5 M_\odot$. The masses range by a factor of ten on either side of this mean value. The high mass end of galactic Giant Molecular Clouds (GMCs) reaches values up to $10^6 M_\odot$ (Solomon *et al.* 1987). From high resolution CO observations of molecular clouds in the arm of M51, Vogel *et al.* (1988) derive masses up to $3 \times 10^7 M_\odot$, referred as Giant Molecular Associations (GMAs). Elmegreen (1994) has recently addressed the formation mechanism of such clouds and found that $10^7 M_\odot$ clouds can be formed due to gravitational instabilities in a spiral arm before the gas flows out of the spiral arm. Thus, depending on the mass of the parent molecular cloud, about 1–10% of the available mass is converted into stars in each episode of star formation.

3.6. Comments on Selected GEHRs

NGC 2363 is left out from most of the above discussions because it is different from the rest of the regions in the sample in terms of its low metallicity and extinction. This region was of special interest in many previous investigations (Peimbert *et al.* 1986, Kennicutt *et al.* 1980). This is one of the regions with the smallest Balmer decrement values. The absence of 2200 Å absorption feature in the *IUE* spectrum (Rosa *et al.* 1985) also suggests a low interstellar extinction towards this region. ϕ/L_B for this region is the highest in the sample. The estimated age is less than 2 Myr, assuming an IMF with slope of 2.5 and $m_u = 60$. Broad band colors for this region are highly contaminated by the strong emission lines (>40% in V and R bands), and hence an investigation regarding the existence of the second population cannot be carried out. Drissen *et al.* (1993) find the kinematic age of the expanding bubble in this region to be 2 Myr. They also found Wolf-Rayet (WR) stars suggesting ages around 3 Myr. It is likely that m_u was close to 120 in this region, with the most massive stars in their WR phase. The inferred mass of the cluster is $4 \times 10^5 M_\odot$.

The starburst nucleus of NGC 5253 has also been well studied using multi-wavelength observations (Walsh & Roy 1989a; Gonzalez-Riestra *et al.* 1987; Moorwood & Glass 1982). The region has sub-solar metallicity. Emission lines contribute around 15–25% in the *BVR* bands. The region agrees very well with the 2-burst model, with the second population just formed. The inferred mass of the embedded stars is $10^5 M_\odot$.

Among the GEHRs in spiral arms, the most interesting complex is the one lying at the tip of the north-east arm of NGC 2997(N2997NE-G1). The complex contains three knots (denoted by 1, 2, 32 in Paper I) of similar brightness in the continuum light while the knot 32 is totally absent in the Hα image. Knots 1 and 2 are treated as independent regions and are included in our plots. We infer that the knot 1 itself contains stars from more than one burst, with a very young second burst. The bigger aperture measurements containing all the three knots support the results on individual knots. A similar behaviour is also seen in complexes N2997NE-G3 and N2997NE-G4.

3.7 Emission Line and Continuum Peaks of GEHRs

In two of the program galaxies (NGC 2997, 4303), we found a noticeable mismatch of continuum and line emitting peaks significantly larger than the alignment errors. These results are particularly worth the attention, as there was a good agreement of the positions of knots in the *BVR* bands. As noted in Paper I, this mismatch has necessitated us to choose centers and radii of apertures by examining both the broad band and Hα images. We attempted getting a rough estimate of the separations between the emission line and continuum knots in two of the galaxies mentioned above. The measured separation between the peaks of nebular and stellar continuum knots is 42 ± 20 pc for 5 regions in NGC 2997 and 100 ± 37 pc for 13 regions in NGC 4303. It is obvious that the lower limit to the separations is due to the lack of resolution ($\sim$ 18 and 34 pc at the distances of NGC 2997 and 4303). The upper limit to the separation comes from the typical separation of star-forming complexes (chain of H II regions) in spiral arms. The mean separation is 450 ± 100 pc and 1200 ± 475 pc for the two galaxies that we have considered. It is interesting to note that the separation between the neighbouring knots with striking brightness differences are around one tenth of the mean separation between distinct H II complexes. Also, the separation between the nebular and continuum knots that we have obtained are similar to the sizes of the largest Giant Molecular Clouds. This separation is also of the same order as the one between the old and the young populations in 30 Dor (Hyland *et al.* 1992).

In order to explain the photometric properties of H II complexes, we required a population older than 5 Myr superposed on a younger population for a majority of the sample regions. We are tempted to believe that in some cases we have actually resolved these two populations as Hα and continuum knots. If the older population has triggered the formation of younger population, we estimate the speed of propagation of the trigger as 40–100 pc in $\sim$10 Myr, or 4–10 km s^{-1}. This value is reasonable for a trigger in terms of mass-loss driven stellar wind from the older population.

Direct confirmation of these results will require spectroscopy of continuum bright knots for detectable signatures of red supergiants. Images taken at high spatial resolutions, such as possible with the *Hubble Space Telescope* will be invaluable in quantifying the separations with reduced uncertainties.

3.8. Summary of Results

From the discussions above, we draw the following conclusions regarding the extinction and star formation in GEHRs in our sample.

(1) The dereddened colors of the embedded clusters are found to correlate with the visual extinction estimated from the Balmer decrement. Regions having the bluest colors have larger A_v values, implying an over-estimation of reddening towards embedded cluster stars. The fraction g of visual extinction experienced by the stars to that by the nebular gas is estimated to be 0.7 ± 0.2, from a subset of the bluest regions in the sample. The value of g is likely to be even smaller if one considers the various uncertainties in the determination of g. We use a value of $g=0.5$, which is the value derived by Calzetti *et al.* (1994) for nuclear star-forming regions.

(2) GEHRs with a single instantaneous burst of star formation are rare in our sample. Loss of ionizing photons amounting to $\sim$35% is inferred in some regions, which may be explained as caused by the direct absorption by dust, if $m_u=60$. Other mechanisms such as the escape of ionizing photons through lower density regions, or total absorption of some of the Balmer line photons by intervening dust clouds, have to be invoked if $m_u>60$. Escaping Lyman continuum photons possibly ionize the low density inter-stellar medium, thus explaining the origin of extra-H II region ionized gas detected by Hunter & Gallagher (1992).

(3) There is a large scatter in the $B-V$ and $V-R$ colors for a given ϕ/L_B. Adding a population rich in red supergiants, supposedly from an earlier burst, to a young population responsible for ionization, explains all the three observables. 70% of the sample regions are found to be in this phase of star formation. The estimated age of the older population is 10 Myr.

(4) We find the Hα emitting knots spatially separated from the continuum knots in NGC 2997 and 4303, from careful measurements of positions of knots on Hα and broad band images. If we attribute these knots to young and old populations, there is a spatial separation in addition to the age difference between the two populations. A mild trigger induced by mass-loss winds from massive stars of previous generation is a viable mechanism for producing successive generations of starbursts in GEHRs.

(5) The evaluation of IMF parameters namely m_u and α, which are greatly needed in understanding star-formation processes in different environments, is hampered by the uncertainties in g, in quantifying the loss of ionizing photons and by the existence of an older population. The present observations do not compel us to choose an IMF slope far away from the Salpeter's value of 2.35. An upper cut-off of $60M_\odot$ can explain a majority of the regions.

(6) The mass of gas converted to stars in each burst is $10^5M_\odot$, with an order of magnitude spread in mass on either side.

(7) The sample contains many metal-rich regions. It is desirable that stellar evolutionary codes become available at metallicities higher than $2Z_\odot$, considering the heavy dependence of evolution on metallicity.

4. DISCUSSION

In this section we discuss the main results obtained in our work, namely the reduced extinction towards stellar continua and the co-existence of two populations in a majority of the GEHRs, in the context of earlier work on GEHRs and related objects. There have been studies of GEHRs and H II galaxies that show indications of reduced extinction towards stars, although interpreted differently by the authors. We look at those results afresh in the following paragraphs.

4.1. Hβ Equivalent Widths

The most widely used diagnostic parameter for star formation so far is the spectroscopically derived Hβ equivalent width. Viallefond (1987), from his compilations, finds that the Hβ equivalent widths and the effective temperatures of the cluster (defined by the ratio of helium ionizing to hydrogen ionizing photons) cannot be simultaneously explained. He finds the observed Hβ equivalent widths to be lower by a factor of 3–4 compared to models with Salpeter IMF without evolution. This is essentially the same discrepancy that we have found in Figs. 3 and 4, where observed $\log(\phi/L_B)$ values are much lower than the IB models with moderate evolution. Aperture size effects and usage of improper model atmosphere were thought by Viallefond to be partly responsible for the discrepancy. The method followed in the present study takes care of both these effects, but still retains the discrepancy. The data set of Terlevich *et al.* (1991) on H II galaxies also shows the discrepancy as discussed below.

A spectrophotometric catalogue of H II galaxies containing 425 objects is published by Terlevich *et al.* (1991). It is known since the work of Sargent & Searle (1970) that H II galaxies are ionized by massive clusters of coeval OB stars. These galaxies are presently experiencing a high level of star formation activity closely resembling "starburst" galaxies on the higher scale and GEHRs on the lower scale. Observable properties are dominated by young stellar component with little or no evidence for any underlying population (Campbell & Terlevich 1984; Melnick *et al.* 1985). Among other quantities, Terlevich *et al.* publish Hα and Hβ equivalent widths in their catalogue. Like giant extragalactic H II regions these galaxies are also thought to be simpler systems dominated by a young star-forming complex. Thus, the evolutionary population synthesis model discussed in Paper II is valid for these systems as well. As a class, H II galaxies are low metallicity systems and hence we compare the median Hα and Hβ equivalent widths of this sample with our model at $Z=0.1Z_\odot$ metallicity. The computed median Hα and Hβ equivalent widths for the sample regions are 172 Å and 33 Å respectively. These values compare well with models which produce $\log(\phi/L_B)_2$ values close to our median value of -1.75. For the IMF with $m_u=60$ and $\alpha=2.5$ at $Z=0.1Z_\odot$, the IB model corresponds to evolution beyond 5 Myr. Based on the photometry of Huchra (1977) and spectroscopy of Skillman & Kennicutt (1993), we derive $\log(\phi/L_B)_2=-1.74$, $(B-V)_2=-0.02$ and $(V-R)_2=0.13$ for the blue compact galaxy IZw18. These values suggest an instantaneous burst of star formation of age $\sim$5 Myr, which implies that the most recent burst in IZw18 has properties similar to the average properties of H II galaxies. Statistically one expects star-forming regions to be detected at their bright young phase ($\leq$3 Myr). In the entire spectrophotometric catalogue there are only three galaxies which have Hβ equivalent widths >350 Å, the expected value for a cluster younger than 3 Myr.

With our new prescription for extinction correction, Hα and Hβ equivalent widths depend on the extinction, contrary to normal convention. Correction to this effect increases the observed equivalent widths, bringing them closer to the values expected for young clusters. The escape of Lyman continuum photons from the nebula also leads to a decrease in the observed equivalent widths. The addition of evolved stars from previous generations adds to the stellar continuum, thus resulting in the decrease of Balmer line equivalent widths. Thus, the observed low Balmer line equivalent widths in GEHRs and H II galaxies can be explained by a combination of the above processes.

4.2. UV Continuum Observations

Young and massive stars emit most of their energy at UV wavelengths. Thus, the UV continuum serves as a very good tracer of massive star formation. The reduced extinction suffered by the stellar continuum, as we found from optical colors, should be affecting the observed spectra in the UV wavelength regions also. UV part of the spectra are essentially independent of IMF differences and hence are good indicators of extinction. Such spectra have become available only recently through rocket and satellite observations. Results from these UV spectra of GEHRs and other objects are discussed in the following paragraphs.

Rosa *et al.* (1985) have published UV spectra of GEHRs based on the *International Ultraviolet Explorer* (*IUE*) observations. It is found that often the 2200 Å absorption feature is weak or absent, although the optical extinction combined with the galactic extinction law predicts much stronger bump. From the observed bumps in five objects, Rosa *et al.* (1985) infer $E(B-V)$ to be not larger than 0.5 for GEHRs. It should be noted that the $E(B-V)$ value obtained from this method measures the "true" stellar extinction, while that derived from the Balmer decrement measures the extinction towards the gaseous component. These observations again indicate lesser extinction towards stellar continuum compared to the nebular radiation.

M83 was one of the targets for rocket UV imaging by Bohlin *et al.* (1990). The UV images of this galaxy were obtained at 1540 and 2360 Å and aperture photometry was performed on 18 H II regions to get monochromatic magnitudes $m_{\rm fuv}$ and $m_{\rm nuv}$ respectively. They have performed $V,B-V$ photometry based on the images of Talbot *et al.* (1979). By fitting a straight line to the reddened $m_{\rm nuv}-V$ and $m_{\rm fuv}-V$ colors, they find that the reddening curve towards stars in this galaxy is the same as that for our galaxy. The color excesses $E(B-V)$ are derived by comparing the observed $m_{\rm nuv}-V$ colors with a model with Salpeter slope and $m_u=120$, $m_l=1.8$. The mean value of color excess so derived is $E(B-V)=0.25$ with a small scatter (0.05 mag rms). Dufour *et al.* (1980) present optical spectrophotometry of six H II regions in this galaxy apart from the nucleus. The derived $E(B-V)$ values from the Balmer decrement have a median value of 0.75, three times larger than the values estimated from the UV continuum. These observations are again consistent with our findings that the reddening towards stellar component is less than that for the nebular component. Dereddening the colors with the $E(B-V)$ values of Bohlin *et al.* fits with the models with evolution within 2 Myr.

Blue compact galaxies have attracted considerable attention in the UV, because of their expected blue spectrum. Like the study of GEHRs in M83, these galaxies also show much

lesser extinction towards the UV stellar continuum compared to the values expected from the Balmer decrement (Fanelli *et al.* 1988).

Calzetti *et al.* (1994) have recently analyzed *IUE*-UV and the optical spectra of 39 starburst and Blue Compact Galaxies in order to study the average properties of dust extinction in extended regions of galaxies. To date, this is the most exhaustive study on the topic of extinction towards the stellar continuum and nebular radiation in star-forming regions, and hence is the most relevant from the point of view of our study. Calzetti *et al.* find a correlation between the slope of the UV spectrum and the optical depth between the Balmer emission lines Hα and Hβ, which cannot be satisfactorily reproduced by any of the five geometrical distributions of dust they have considered, for both Milky Way and LMC extinction laws. They derive an extinction law directly from the data in the UV and optical spectral range. The resulting curve is characterized by an overall slope which is more gray compared to the Milky Way extinction law, and by the absence of the 2200 Å dust feature. With the new extinction law, the difference in optical depths between Hα and Hβ stellar continua is only half of the difference between the optical depths for the corresponding emission lines. Our results on GEHRs, based on colors, are consistent with these results.

From the above discussions it is evident that the star-forming complexes share the same extinction properties irrespective of spatial scale and strength of star formation or position of the star-forming site in a galaxy. As a rule the stellar continuum in optical and UV regions suffers lesser amount of extinction compared to the radiation from the surrounding nebula. It is likely that the same physical process controls the extinction in all star-forming regions.

4.3. Thermal Radio Emission

The extinction towards a nebula can be derived by using the observed intensity ratio of thermal radio emission to Balmer lines (A_v(radio)). Most often the extinction is measured using two or more of the Balmer lines (A_v(Bal)). Several groups have compared the extinction derived from these two methods (Israel & Kennicutt 1980, Viallefond *et al.* 1982, Caplan & Deharveng 1986). General conclusion from these studies is that A_v(radio) is around 1 mag greater than A_v(Bal). Practically it is often difficult to match the apertures for radio and optical measurements, which might explain a part of the uncertainty in the above conclusions. However, it is believed that the observed higher value of A_v(radio) is real and may be related to the distribution of dust between the source and the observer. Caplan & Deharveng (1986) investigated various dust configurations to explain radio and optical extinction in a sample of H II regions in the LMC. From these they conclude that a uniform extinction cannot explain the LMC data. Some of the extinction is due to clumped dust, well outside of the emission zone, and the rest is caused by dust located closer to or mixed with the ionized gas, where scattering effects are important. Measurement of extinction directly from resolved stars indicates that there is interstellar dust, quite irregularly distributed. Higher extinction from radio measurements implies that some of the Balmer photons are totally absorbed by the intervening dust. Under these conditions, the Lyman continuum luminosity as measured from Balmer lines underestimates the actual ionizing radiation. The fraction f (or more precisely η_{esc} defined in section *3.2*) has a contribution from these undetectable Hα photons. The absolute value of f critically depends on the chosen m_u and hence the estimation of the missing number of ionizing photons cannot be made accurately even if one derives Lyman continuum luminosities from thermal radio continuum.

4.4. The 30 Doradus Complex in LMC

The Tarantula or 30 Dor nebula in the LMC is the closest example of a GEHR. Its relatively nearby location has helped its observation in a great detail. The near-infrared observations revealed the existence of two populations of stars (red and blue) in this complex (McGregor & Hyland 1981). More recently Hyland *et al.* (1992) have surveyed the region to deeper limits ($K=13$ mag) and the earlier results are confirmed. The red population is explained to be corresponding to the red supergiant phase of stars with mass $>20M_\odot$ formed about 20 Myr ago. The older population is spatially separated from the younger one by distances of the order of tens of pc. Hyland *et al.* suggest that the younger cluster has formed due to the collision of the parent cloud with the mass-loss wind of the older cluster stars. The present work has brought out the evidence for such supergiants in a majority of extragalactic H II regions.

5. PROPOSED SCHEME OF STAR FORMATION IN GEHRS

In this section, we propose a scheme of star formation, consistent with all the observed properties of GEHRs. The main results which the model tries to explain are the following.

5.1. Observational Facts

1. The brightest GEHRs in galaxies, often preferred for detailed spectroscopic study, are very rarely found to be genuinely young with only one generation of stars.

2. Among the fainter GEHRs in galaxies, there are a few with very high Hα emission equivalent widths (see Paper I).

3. Hα bright regions in galaxies often contain red supergiants, possibly from an earlier burst ($\sim$10 Myr ago) of star formation.

4. The optical and ultraviolet continua from stars experience lesser amount of extinction compared to radiation from the ionized gas.

5. Some of the neighbouring emitting knots have marked variation in the ratio of Hα to optical continuum.

6. On an average GEHRs contain about $10^5M_\odot$ of stellar mass in each burst.

5.2. Proposed Model

A scenario of propagating star formation in galactic molecular clouds was discussed by Lada (1985). We extend this model to a larger scale to explain the star formation process in GEHRs. To start with, we summarize the known physical properties of GEHRs and the parent molecular clouds. GEHRs show a core-halo morphology in emission lines, with densities decreasing from around 100 cm^{-3} in the core to 1 cm^{-3} in the halo. Kennicutt (1984) points out that the density in the halo almost equals the density of the general ISM. The average sizes of core and halo are around 75 pc and 250 pc, respectively (Sandage & Tammann 1974). In comparison, Galactic GMCs from which stars form have average dimensions of 60 pc (Solomon *et al.* 1987), which is of the order of the dimension of cores of GEHRs. Interestingly, the Giant Molecular Associations found in the spiral arms of M51 (Rand 1993) have also dimensions matching that of halos, though their average densities are higher than the observed densities of GEHR halos. It is likely that GMAs contain a few GMC-like condensations, surrounded by an extended low density inter-clump medium, which get transformed into core and halo respectively after massive stars are formed. An examination of individual regions indicate higher extinction towards higher Hα surface brightness regions (for example see NGC5461 in McCall *et al.* 1985). Thus, the core in an H II complex contains more dust than the surrounding low surface brightness halo. Emission line equivalent widths of Balmer lines seem to be higher near the core compared to the value obtained by integrating over the entire complex, implying that the stars are spread over a larger spatial extent compared to the line emitting cores of GEHRs (Roy *et al.* 1989). Stars, when born, are confined to the highest density regions, thus coinciding with the position of the Hα core. However, the relative velocity of stars with respect to the cloud make them diffuse out of the core into the lower density regions in a few million years (Leisawitz & Hauser 1988).

With the above description of the physical properties of GEHRs and molecular clouds, the overall process of star formation can be divided into four phases, each with a distinct observable signature. These four phases are schematically depicted in Fig. 9. The outer boundary denotes the parent molecular cloud, whose dimension is around 300 pc. The GEHR core is shown by the circle, with the bigger concentric circle denoting the extent of the ionized halo. Stars are denoted by asterix. The irregular pattern indicates the density inhomogeneities in the parent cloud. The approximate time period in each phase is indicated.

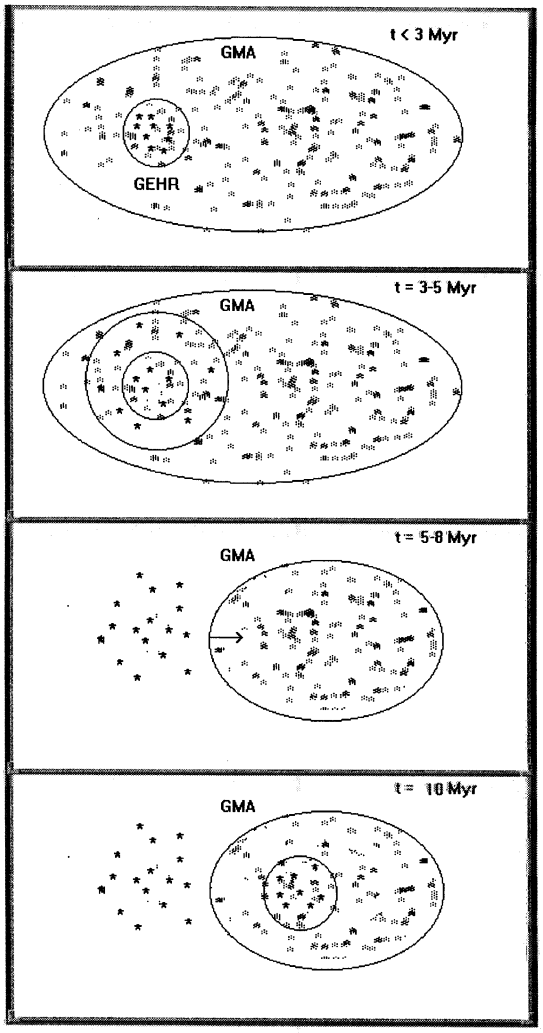

FIG. 9. A schematic diagram of the four phases during star-formation in GEHRs. The outer boundary in each sketch represents a Giant Molecular Association which contains a GEHR, surrounded by the low density gas. The GEHR itself contains cluster stars, clumpy gas and dust as shown. The formation of GEHR core, subsequent formation of the halo, the spreading out of optically luminous stars into lower density regions, and subsequent triggering of a second burst of star formation in the left out gas are some of the salient features of the model. Typical time scales involved are marked on the top right. See section *5.2* for details.

Phase 1: We assume the GEHRs to form in Giant Molecular Associations, which contain several regions of higher than average densities. Some of these condensations grow into GMC-like structures, the densest of which collapses to form stars. This results in an ionization of the high density gas in the immediate vicinity, forming the core of the GEHR. Dust associated with the molecular cloud offers considerable optical extinction, allowing only a few of the young regions to be detected optically as faint Hα emitting knots with weak or no continuum. Regions with high Hα equivalent widths are in this phase of evolution. The large extinction when the cluster is young, makes its optical detection very difficult. τ_B^c is expected to be equal to τ_B^l in the very early phase, with a tendency for τ_B^c to decrease as some of the optically luminous stars diffuse to low density regions. The ionization front is advancing into low density regions. This phase might last for 3 Myr at the most.

Phase 2: There might be a net reduction in the extinction towards a GEHR in a few million years, as the energetic events associated with star formation destroy the dust particles in the core. The reduced extinction makes these regions

optically visible for the first time. Embedded cluster stars might experience additional reduction in extinction as more and more stars diffuse out of the high density cores. By this time the ionization front has also advanced past the high density regions of the molecular cloud, thus creating an extended low density ionized halo, which can be detected only through sensitive observations. This might lead to an underestimation of the ionizing photons. However, emission from the core still dominates the total Balmer emission from the region. Under this configuration, photons from ionized gas encounter more dust clumps, compared to stellar photons. Thus, the stellar continuum experiences lesser extinction compared to radiation from the ionized gas ($\tau_B^c < \tau_B^l$). This phase might continue up to around 5 Myr. The second sketch in Fig. 9 depicts this stage.

Phase 3: The onset of this phase is characterized by the appearance of luminous red and/or blue supergiant stars in the cluster, as the massive stars evolve off the main sequence in around 5 Myr. The cluster appears brightest in the stellar continua from ultraviolet to near-infrared during this phase. This luminous period continues until all the massive stars go through the red supergiant phase ($\sim$12 Myr). In this phase the region is very faint in Hα.

Massive stars lose a large amount of mass and energy during their lifetime, both on and off the main sequence. This results in an increased pressure on the gas left behind after the initial burst of star formation, thus creating another density condensation in the same GMA. Evidence is accumulating for the presence of left over molecular gas in the vicinity of GEHRs (e.g., NGC604 in M33: Israel *et al.* 1990; Wilson & Scoville 1992). The shocked layer starts collapsing, eventually forming a new generation of stars. The delay between the onset of collapse and generation of new stars is given by (Elmegreen 1992),

$$t_{\rm delay} = 2.4 \left(\frac{M}{10^5} \right)^{0.25} \ {\rm Myr}. \qquad (17)$$

For a cloud of mass $10^6 M_\odot$ participating in the collapse this corresponds to $t_{\rm delay} = 4.3$ Myr. The arrow in the third panel indicates that the cloud is collapsing.

Phase 4: The end of phase 3 and the beginning of phase 4 are characterized by the birth of the second generation of massive stars in the same parent molecular cloud. Typically this happens at around 8 Myr, with the exact epoch depending on the mass of the parent cloud and the onset of collapse. During this phase, the region becomes brighter again in H α. By this time the stars from the first generation have evolved, and the cluster itself has moved into regions of lesser extinction. In this phase, the bulk of observed stellar continuum originates from the older generation and hence suffers lesser extinction compared to the ionized gas situated in dense regions, thus continuing the trend shown in Phase 2. GEHRs are expected to be in this phase at about 10 Myr since the beginning of the first generation of stars. For typical propagation speeds ($\sim$10 km s^{-1}), the separation between the two populations amounts to $\sim$100 pc. Thus the two generations of stars can be distinguished, under good spatial resolutions, as neighboring Hα and continuum (stellar) peaks.

In this study, we restricted the evolution of GEHRs up to the second generation. In reality, star formation might continue until the parent clouds of GEHRs are fully disrupted by the energetic events such as multiple supernova explosions. It is likely that bigger systems like H II galaxies and central regions of galaxies experience several bursts of star formation before the consumption of gas is complete. However, the process of formation of multiple bursts might be different in these bigger systems. Recently, Korchagin *et al.* (1995) have constructed propagating star-formation models for the nuclear hot-spots in galaxies and found the star formation lasting for a few tens of million years.

Before building on the above tentative model, it is important to establish the different phases by elaborate observations. This would involve a detailed study of selected high Balmer equivalent width regions to establish that they are young and also that their stellar continuum experiences similar extinction as the radiation from the ionized gas. Regions in the present sample with definite indication of older generation should be observed for the signatures of red supergiants. GEHRs should be imaged in the optical emission and continuum bands with high spatial resolutions, in order to directly resolve the spatially separated generations of stars, one bright in the emission line and the other bright in the stellar continuum. As all these observations are well within the observing capabilities of most medium-sized optical-infrared telescopes, we hope that the above model will be put to test soon.

6. CONCLUSIONS

We find an evidence for reduced extinction towards stellar continuum compared to the extinction derived from the Balmer decrement. Genuinely young GEHRs containing stars from only one generation seem to be very rare in the present sample. Instead, the young and moderately evolved regions contain an older population rich in red supergiants. All these observational facts are put together resulting in a simple qualitative model, which can be tested by a detailed study of selected regions. In the model, GEHRs are obscured by the dust associated with the high density gas when they are young, and are detected only when the stars have moved out of the highest density regions. This leads to a lower effective optical depth towards the stellar continua compared to the emission lines from the ionized gas, whenever GEHRs are detected. The mass-loss wind from the massive stars triggers a second burst of star formation in the parent cloud, providing a fresh input of ionizing radiation. The presence of stars from two bursts and reduced net extinction makes these regions easily noticeable on galaxy images, and hence are preferred regions in most of the studies. Star formation in GEHRs stops after two or more bursts, probably because of disruption of the parent gas cloud.

The suggestions made by the referee Marshall L. McCall has helped enormously in improving the paper, especially in revising the proposed model for star-formation.

REFERENCES

Alloin, D., Edmunds, M. G., Lindbland, P. O., & Pagel, B. E. G. 1981, A&A, 101, 377
Belfort, P., Mochkovitch, R., & Dennefeld, M. 1987, A&A, 176, 1
Bohlin, R. C., Cornett, R. H., Hill, J. K., & Stecher, T. P. 1990, ApJ, 363, 154
Bottinelli, L., Gougenheim, L., Paturel, G., & de Vaucouleurs, G. 1984, A&AS, 56, 381
Calzetti, D., Kinney, A. L., & Storchi-Bergmann, T. 1994, ApJ, 429, 582
Campbell, A. W., & Terlevich, R. J. 1984, MNRAS, 211, 15
Caplan, J., & Deharveng, L. 1986, A&A, 155, 297
Cerviño, M., & Mas-Hesse, J. M. 1994, A&A, 284, 749
de Vaucouleurs, G. 1979, AJ, 84, 1270
de Vaucouleurs, G., de Vaucouleurs, A., Corwin, H. G., Buta, R., Patural, G., & Fouqué, P. 1991, Third Reference Catalogue of Bright Galaxies (Springer, New York) (RC3)
Drissen, L., Roy, J.-R., & Moffat, A. F. J. 1993, AJ, 106, 1460
Dufour, R. J., Talbot, R. J., Jensen, E. B., & Shields, G. A. 1980, ApJ, 236, 119
Elmegreen, B. G. 1992, in Star Formation in Stellar Systems, edited by G. Tenorio-Tagle, M. Prieto, and F. Sánchez (Cambridge University Press, Cambridge), p.413
Elmegreen, B. G. 1994, ApJ, 433, 39
Fanelli, M. N., O'Connell, R. W., & Thuan, T. X. 1988, ApJ, 334, 665
Gonzalez-Riestra, R., Rego, M., & Zamorano, J. 1987, A&A, 186, 64
Huchra, J. P. 1977, ApJS, 35, 171
Humphreys, R. M., & McElory, D. B. 1984, ApJ, 284, 565
Hunter, D. A., & Gallagher, J. S. 1992, ApJL, 391, L9
Hunter, D. A., Hawley, W.M., & Gallagher, J.S. 1993, AJ, 106, 1797
Hyland, A. R., Straw, S., Jones, T. J., & Gatley, I. 1992, MNRAS, 257, 391
Israel, F. P., Hawarden, T. G., & Geballe, T. R. 1990, MNRAS, 242, 471
Israel, F. P., & Kennicutt, R. C. 1980, ApJ, 21, L1
Jones, J. E., & Jones, B. J. T. 1980, MNRAS, 191, 685
Kennicutt, R. C. 1979, ApJ, 228, 394
Kennicutt, R. C. 1981, ApJ, 247, 9
Kennicutt, R. C. 1984, ApJ, 287, 116
Kennicutt, R. C., Balick, B., & Heckman, T. 1980, PASP, 92, 134
Korchagin, V. I., Kembhavi, A. K., Mayya, Y. D., & Prabhu, T. P. 1995, ApJ, 446, 574
Kurucz, R. L. 1992, in Stellar Populations of Galaxies, IAU Symposium No. 149, edited by B. Barbuy and A. Renzini (Kluwer, Dordrecht), p.225
Lada, C. J. 1985, in Star Forming Regions, IAU Symposium No. 115, edited by M. Peimbert and J. Jugaku (Reidel, Dordrecht), p.1
Leisawitz, F., & Hauser, M.G. 1988, ApJ, 332, 954
Leitherer, C., & Heckman, T.M. 1995, ApJS, 96, 9
Lequeux, J., Maucherat-Joubert, M., Deharveng, J. M., & Kunth, D. 1981, A&A, 103, 305
Mas-Hesse, M., & Kunth, D. 1991, A&AS, 88, 399
Mayya, Y. D. 1994, AJ, 108, 1276 (Paper I)
Mayya, Y. D. 1995, AJ, 109, 2503 (Paper II)
McCall, M. L., Rybski, P. M., & Shields, G. A. 1985, ApJS, 57, 1
McGregor, P. J., & Hyland, A. R. 1981, ApJ, 250, 116
Melnick, J., Terlevich, R., & Moles, M. 1985, RMxA&A, 11, 91
Mezger, P. G. 1978, A&A, 70, 565
Moorwood, A. F. M., & Glass, I. S. 1982, A&A, 115, 84
Osterbrock, D. E. 1989, Astrophysics of Gaseous Nebulae and Active Galactic Nuclei (University Science Books, California)
Parker, J. Wm., & Garmany, C. D. 1993, AJ, 106, 1471
Peimbert, M., Peña, M., & Torres-Peimbert, S. 1986, A&A, 158, 266
Peterson, C. J. 1978, ApJ, 226, 75
Rand, R. J. 1993, ApJ, 404, 593
Rosa, M., Joubert, M., & Benvenuti, P. 1985, A&AS, 57, 361
Roy, J.-R., & Walsh, J. R. 1987, MNRAS, 228, 883
Roy, J.-R., & Walsh, J. R. 1988, MNRAS, 234, 977
Roy, J.-R., Belly, J., & Walsh, J. R. 1989, AJ, 97, 1010
Salpeter, E. E. 1955, ApJ, 121, 161
Sandage, A. R., & Tammann, G. A. 1974, ApJ, 190, 525
Sandage, A. R., & Tammann, G. A. 1976, ApJ, 210, 7
Sandage, A. R., & Tammann, G. A. 1981, A Revised Shapley-Ames Catalog of Bright Galaxies (Carnegie Institution, Washington)
Sargent, W. L. W., & Searle, L. 1970, ApJ, 162, L155
Scalo, J. M. 1986, Fund. of Cosmic Phys., 11, 1
Scalo, J. M. 1987, in Starbursts and Galaxy Evolution, edited by T. X. Thuan, T. Montmerle, and J. T. T. Van (Editions Frontieres, Gif sur Yvette), p.445
Schaerer, D., Charbonnel, C., Meynet, G., Maeder, A., & Schaller, G. 1993, A&AS, 102, 339
Schaller, G., Schaerer, G., Meynet, G., & Maeder, A. 1992, A&AS, 96, 269
Seaton, M. J. 1979, MNRAS, 187, 73P
Shields, G. A. 1990, ARA&A, 28, 525
Shields, G. A., Skillman, E. D., & Kennicutt, R. C. 1991, ApJ, 371, 82
Skillman, E. D., & Kennicutt, R. C. 1993, ApJ, 411, 655
Smith, L. F., Biermann, P., & Mezger, P. G. 1978, A&A, 66, 65
Solomon, P. M., Rivolo, A. R., Barrett, J., & Yahil, A. 1987, ApJ, 319, 730
Talbot, R. J., Jensen, E. B., & Dufour, R. J. 1979, ApJ, 229, 91
Terlevich, R., Melnick, J., Masegosa, J., Moles, M., & Copetti, M. V. F. 1991, A&AS, 91, 285
Viallefond, F. 1987, Ph.D. thesis, University of Paris
Viallefond, F., Goss, W. M., & Allen, R. J. 1982, A&A, 115, 373
Vogel, S. M., Kulkarni, S. R., & Scoville, N. 1988, Nature, 334, 402
Walsh, J. R., & Roy, J.-R. 1989a, MNRAS, 239, 297
Walsh, J. R., & Roy, J.-R. 1989b, ApJ, 341, 722
Wilson, C. D., & Scoville, N. 1992, ApJ, 385, 512